Selective Isotope CT Imaging Based on Nuclear Resonance Fluorescence Transmission Method

AUTHOR(S):

Ali, Khaled; Ohgaki, Hideaki; Zen, Heishun; Kii, Toshiteru; Hayakawa, Takehito; Shizuma, Toshiyuki; Toyokawa, Hiroyuki; ... Ur, Calin Alexandru; Fujimoto, Masaki; Katoh, Masahiro

CITATION:

Ali, Khaled ...[et al]. Selective Isotope CT Imaging Based on Nuclear Resonance Fluorescence Transmission Method. IEEE Transactions on Nuclear Science 2020, 67(8): 1976-1984

ISSUE DATE:

2020-08

URL:

http://hdl.handle.net/2433/254063

Selective Isotope CT Imaging Based on Nuclear Resonance Fluorescence Transmission Method

Khaled Ali, *Student Member, IEEE*, Hideaki Ohgaki, *Member, IEEE*, Heishun Zen, Toshiteru Kii, Takehito Hayakawa, Toshiyuki Shizuma, Hiroyuki Toyokawa, Yoshitaka Taira, Violeta Iancu, Gabriel Turturica, Călin Alexandru Ur, Masaki Fujimoto, and Masahiro Katoh

***Abstract*— The isotope selectivity of computed tomography (CT) imaging based on nuclear resonance fluorescence (NRF) transmission method using a quasi-monochromatic laser Compton scattering (LCS) gamma-ray beam in the MeV region was demonstrated at the Ultra Violet Synchrotron Orbital Radiation–III (UVSOR-III) Synchrotron Radiation Facility (Institute of Molecular Science, National Institute of Natural Science) for two enriched lead isotope rods (^{206}Pb and ^{208}Pb) implanted in an aluminum cylinder. Since these two rods show the same gamma-ray attenuation in atomic processes, it is impossible to differentiate between them using a standard Gamma-CT technique based on atomic attenuation of gamma rays. The LCS gamma-ray beam had a maximum energy of 5.528 MeV and an intensity of approximately 5.5 photons/s/eV at the resonance energy ($J^{\pi} = 1^{-}$ at 5.512 MeV in ^{208}Pb). A lead collimator with a hole diameter of 1 mm was used to define the size of the LCS gamma-ray beam at the CT target. The CT image of the ^{208}Pb rod was selectively obtained with a 2-mm pixel size resolution, which was determined by the horizontal step size of the CT stage.**

***Index Terms*— Computed tomography (CT), isotope distribution, laser Compton scattering (LCS) gamma-ray beam, nuclear resonance fluorescence (NRF).**

I. Introduction

NONDESTRUCTIVE assay (NDA) technology, which is used to identify specific isotopes in a substance, plays a critical role in nuclear safety [1], [2], nuclear waste management [3], and nonproliferation of nuclear materials [4], [5]. Bertozzi *et al.* [1] proposed the nuclear resonance fluorescence (NRF) process [6] with Bremsstrahlung gamma-ray beams for the measurement of the isotopes of interest. Fig. 1 shows the schematic diagram of the NRF process. If the energy of an incident gamma ray is nearly identical to the excitation energy of an isotope of interest, the isotope is excited and subsequently decays either to the ground state or to an excited state through the emission of a gamma ray. The energy dependence of the NRF cross section is described by the Breit–Wigner resonance [7], [8]. Owing to the dependence of the excitation energies on the nuclear species (isotope), the NRF assay can provide isotope-specific signatures for many materials [1]. NDA using NRF with a quasi-monochromatic gamma-ray beam generated through laser Compton scattering (LCS) on relativistic electron beams has been proposed previously [2], [3]. The LCS gamma-ray beam [9], [10] is characterized by properties such as energy tunability, quasi-monochromatic energy spectrum, controllable polarization, and strong directionality [11]–[13]. Kikuzawa *et al.* [14] performed a proof-of-principle experiment of NDA by using NRF gamma rays from the lead in an iron box with a thickness of 1.5 cm irradiated by an LCS gamma-ray beam with a high signal-to-noise ratio. LCS gamma-ray beams in the MeV energy region are currently available for basic research and applications at the high intensity gamma-ray source (HIγS) [11], New SUBARU [12], and Ultra Violet Synchrotron Orbital Radiation–III (UVSOR-III) [15].

A method called "transmission method" or "notch detection method," illustrated in Fig. 2, has been proposed for NDA measurements of the isotopes of interest [1], [6]. Resonance widths, typically ∼1 eV after Doppler broadening, are considerably narrower than the energy width of an incident gamma-ray beam, with the absorption of gamma rays by nuclear resonance occurring only in the nuclide of interest [7]. When an isotope of interest is already present in the measured sample [computed tomography (CT) target shown in Fig. 2], the spectral flux of the transmitted photons at the resonant energy decreases due to resonant absorption, leading to a narrow and sharp dip (called a notch) in the transmitted gamma-ray energy spectrum [16]. When the transmitted gamma ray irradiates the witness target that includes the same isotope of interest, gamma rays are emitted from the isotope via the NRF process. The NRF yield from the witness target is the negative exponential function of the amount of isotope in the CT sample along the beam path. CT is an imaging technique used to

Manuscript received March 13, 2020; revised May 29, 2020; accepted June 18, 2020. Date of publication June 24, 2020; date of current version August 14, 2020. This work was supported by the Japanese Sociality for the Promotion of Science (JSPS) KAKENHI under Grants JP18H01916, 18H03715, and 17K05482.

Khaled Ali, Hideaki Ohgaki, Heishun Zen, and Toshiteru Kii are with the Institute of Advanced Energy (IAE), Kyoto University, Kyoto 611-0011, Japan (e-mail: khaled.ali.28e@st.kyoto-u.ac.jp; ohgaki.hideaki.2w@kyoto-u.ac.jp; zen@iae.kyoto-u.ac.jp; kii@iae.kyoto-u.ac.jp).

Takehito Hayakawa and Toshiyuki Shizuma are with the Tokai Quantum Beam Science Center, National Institutes for Quantum and Radiological Science and Technology (QST), Naka 319-1106, Japan (e-mail: hayakawa.takehito@qst.go.jp; shizuma.toshiyuki@qst.go.jp).

Hiroyuki Toyokawa and Yoshitaka Taira are with the National Institute of Advanced Industrial Science and Technology (AIST), Tsukuba 3058568, Japan (e-mail: h.toyokawa@aist.go.jp; yoshitaka-taira@aist.go.jp).

Violeta Iancu, Gabriel Turturica, and Călin Alexandru Ur are with the Extreme Light Infrastructure—Nuclear Physics, Horia Hulubei National Institute for Research and Development in Physics and Nuclear Engineering, 077125 Măgurele, Romania (e-mail: violeta.iancu@eli-np.ro; gabriel.turturica@eli-np.ro; calin.ur@eli-np.ro).

Masaki Fujimoto is with the National Institute of Natural Science, Institute of Molecular Science, Ultra Violet Synchrotron Orbital Radiation (UVSOR) Synchrotron Radiation Facility, Okazaki 444-8585, Japan (e-mail: fmoto@ims.ac.jp).

Masahiro Katoh is with the National Institute of Natural Science, Institute of Molecular Science, Ultra Violet Synchrotron Orbital Radiation (UVSOR) Synchrotron Radiation Facility, Okazaki 444-8585, Japan, and also with the Hiroshima Synchrotron Radiation Center, Hiroshima University, Higashihiroshima 739-0046, Japan (e-mail: mkatoh@ims.ac.jp).

Color versions of one or more of the figures in this article are available online at http://ieeexplore.ieee.org.

Digital Object Identifier 10.1109/TNS.2020.3004565

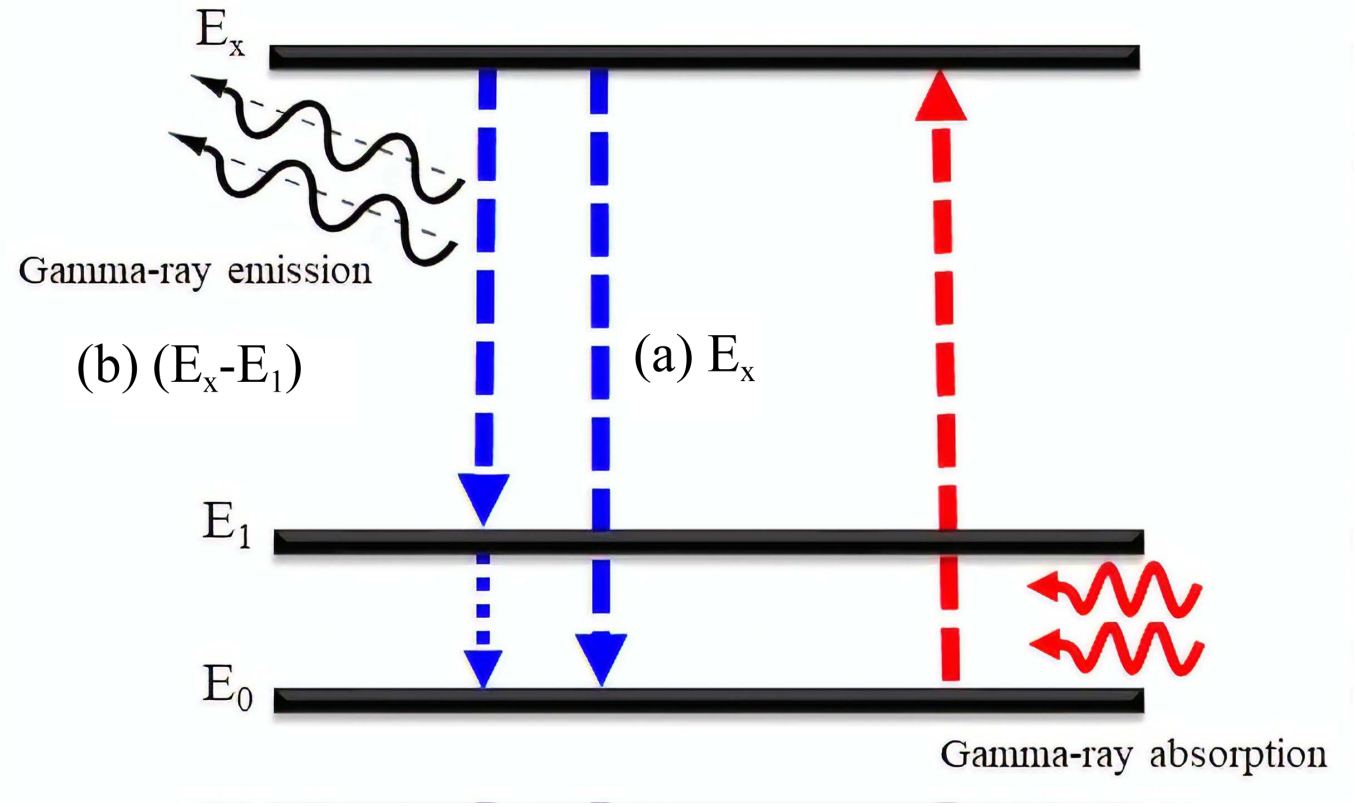

Fig. 1. Schematic of the NRF process, which involves the resonant excitation of the nucleus via the absorption of gamma rays with energy equal to the excitation energy (E_x). The nucleus then de-excites by the emission of gamma rays with (a) energy (E_x) back to the ground state or (b) energy ($E_x - E_1$) to an excited state with energy E_1.

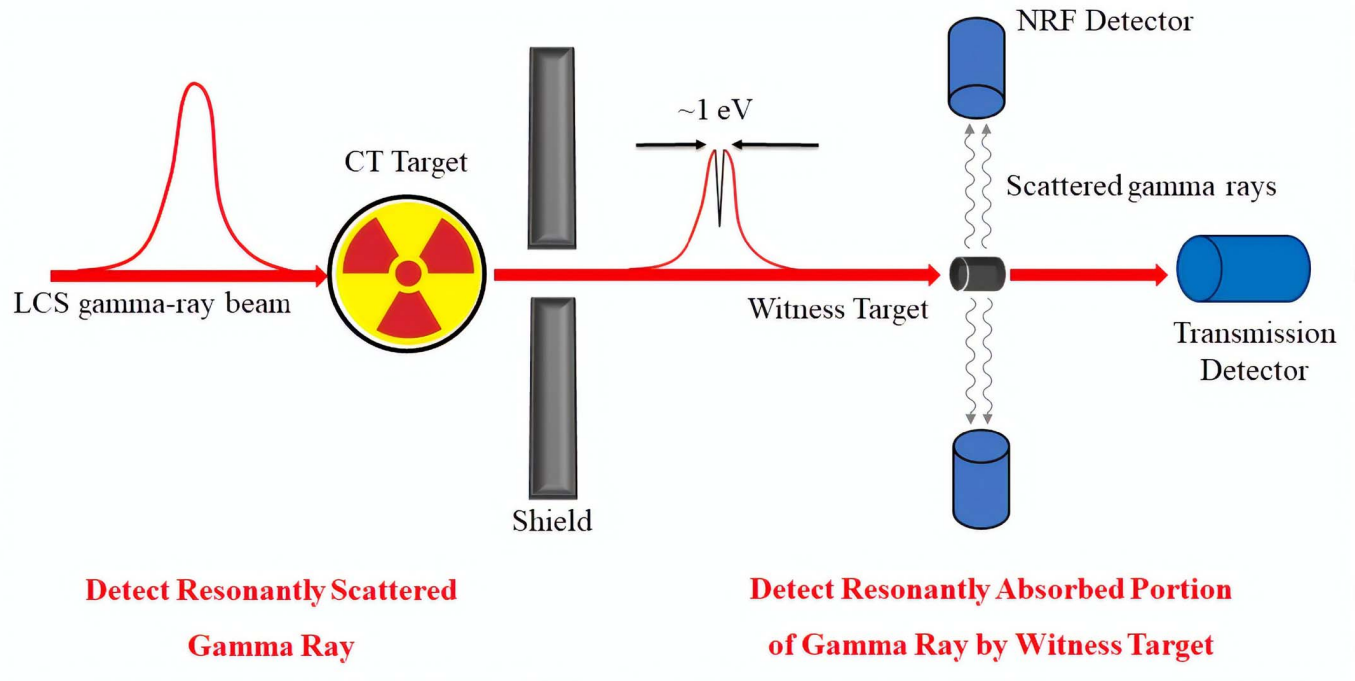

Fig. 2. NRF transmission method.

reconstruct the cross-sectional image of a sample from several projections acquired at different projection angles. Gamma-ray CT scanners are employed in various medical fields [17] and for nondestructive industrial inspections [18], [19].

CT can be integrated with the NRF transmission method, known as NRF-CT, to obtain isotope-specific CT images using gamma rays in the MeV energy region [20], [21]. One of the remarkable features of NRF-CT is that the isotope of interest

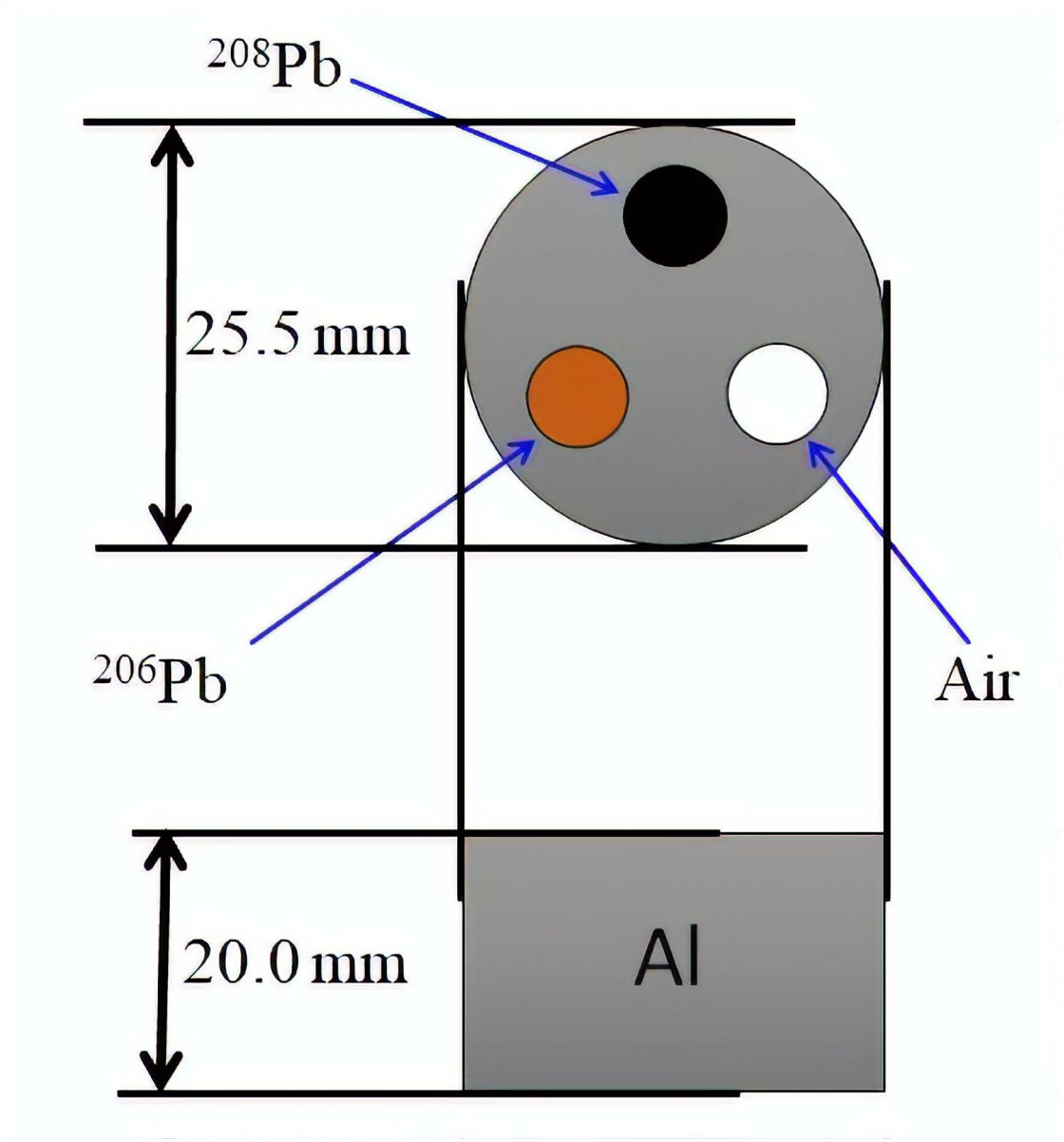

Fig. 3. Geometry of the CT target, which consisted of a cylindrical aluminum retainer with a diameter of 25 mm and a height of 20 mm. The retainer had three holes with equal diameters of 6.1 mm and pitch angle of 120°. The enriched lead isotope rods (^{206}Pb and ^{208}Pb) were placed in two of the holes, while the third hole was left empty.

can be selectively identified from a sample containing several isotopes. Zen *et al.* [16] demonstrated an image of a ^{208}Pb isotope in the natural lead, with a pixel size of 5 mm in the resolution. The CT target consisted of a natural lead rod implanted in an iron cylinder filled with aluminum (Al), with an iron rod and air (hole).

The aim of this study was to demonstrate the isotope selectivity of NRF-CT imaging using two different isotope-enriched lead rods (^{206}Pb and ^{208}Pb). Because these two rods exhibit the same gamma-ray attenuation in atomic processes, it is impossible to distinguish the two rods using a standard CT technique based on the atomic attenuation of gamma rays. We employed an upgraded laser system that could generate a tenfold intensity of the LCS gamma-ray beam when compared to the previous system [16]. The energy of the gamma-ray beam was increased to enable excitation at 5.512 MeV, as the NRF cross section was two times larger than that at 5.292 MeV in previous work [16]. An increased number of data points were measured using an LCS beam with a smaller diameter of 1 mm and a scanning step of 2 mm to obtain a CT image with a higher spatial resolution than the previous work [16].

II. Experimental Procedure

In this study, the experiments were performed at the BL1U beamline located at the UVSOR-III Synchrotron Radiation Facility [15], [22]. The developed NRF-CT system was based on a first-generation CT scanner [23]. Fig. 3 shows the structure of the CT target. A cylindrical aluminum holder with a diameter of 25 mm and a height of 20 mm was used as the specimen holder. The specimen holder consisted of three circular holes each with a diameter of 6.1 mm with an equal pitch angle of 120°. Two enriched lead isotope rods (^{206}Pb in purity $>$93.3% with not more than 1% of ^{208}Pb and ^{208}Pb in purity $>$97.8% with not more than 1% of ^{206}Pb) were used in the experiment. Each rod was cylindrical with a diameter of 6 mm, height of 18 mm, and weight of 6 g. The two

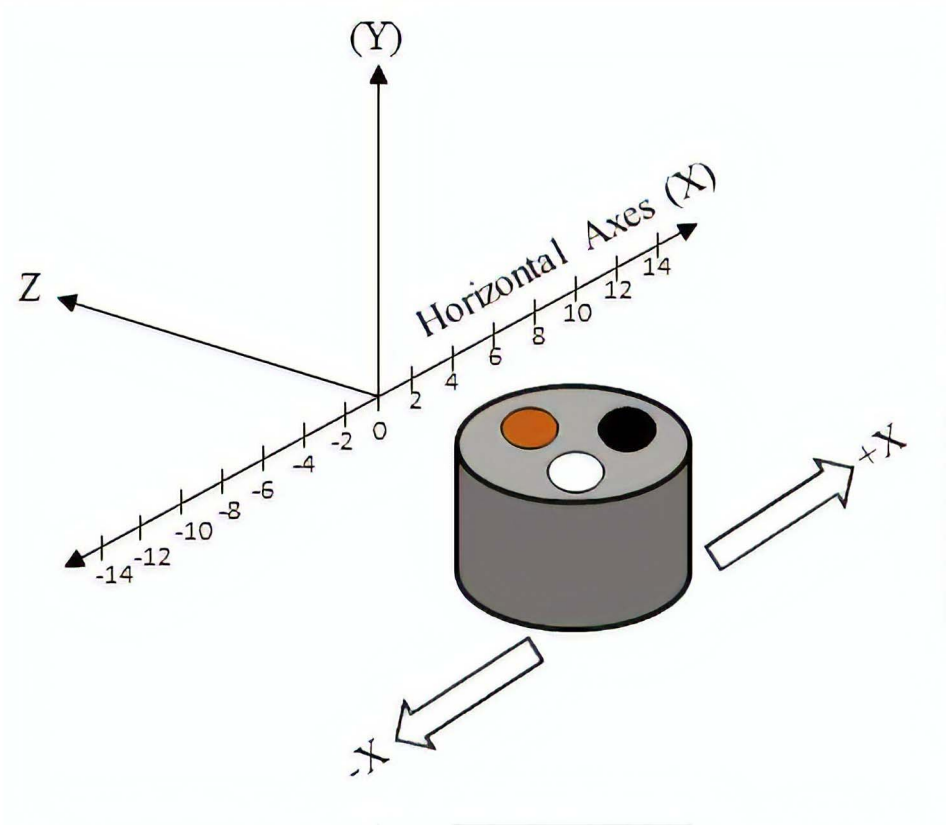

Fig. 4. Acquisition geometry of the CT target in the horizontal direction (x). The position of the CT target was varied from −14 to 14 mm in steps of 2 mm within the movement range.

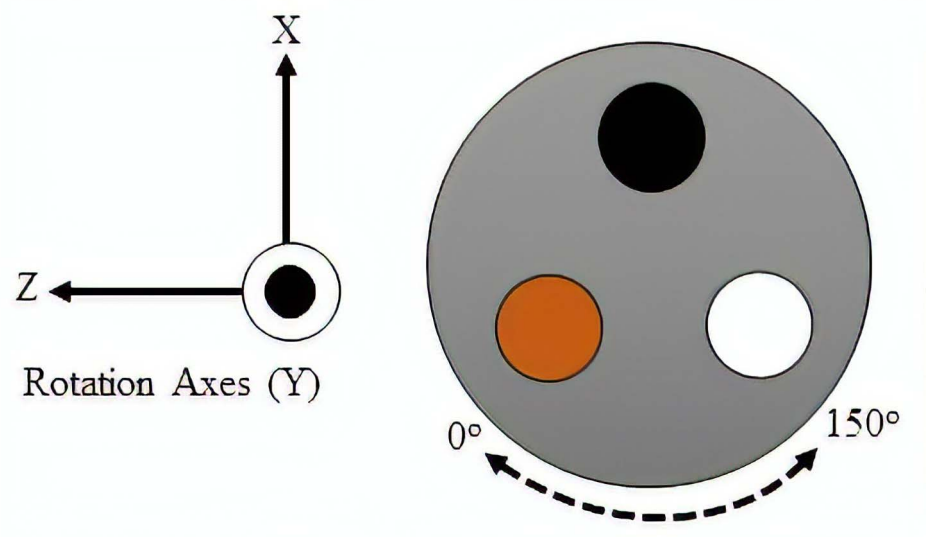

Fig. 5. Acquisition geometry of the CT target in the direction of rotation (θ). The CT target was rotated in steps of 30° in the range of 0°–150° around the Y-axis.

lead isotope rods were placed in two holes of the specimen holder, while the third hole was left empty. The CT target positioned on a two-axis moving stage was scanned along the horizontal dimension (x) with a step size of 2 mm in the range of −14 to 14 mm, as shown in Fig. 4. The acquisition was also performed in the direction of rotation (θ), in which the CT target rotated in steps of 30° in the range of 0°–150° around the y-axis, as shown in Fig. 5. In addition to one acquisition without the CT target, 90 data points with the CT target were acquired (15 steps along the horizontal axes × 6 angles of rotation). The averaged measurement time for one data point was approximately 40 min.

We used a Tm-fiber laser system (TLR-50-AC-Y14, IPG Laser GmbH) with the maximum average power of 50 W, which was ten times as large as that of the previously employed laser system [16]. We operated it in a continuous

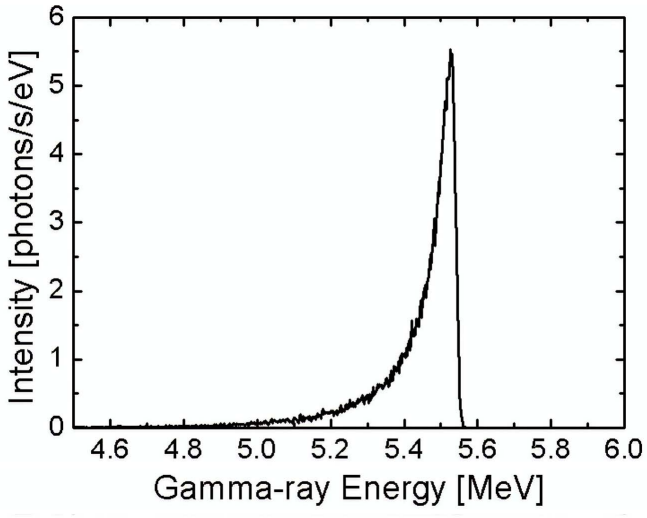

Fig. 6. Expected LCS gamma-ray spectrum obtained with a collimator hole diameter of 1-mm using EGS5 Monte Carlo simulations for an LCS gamma-ray flux of 1×10^8 photons/s.

wave (CW) operation mode with random polarization. The laser wavelength of 1.896 ± 2 μm (0.6539 eV) can generate the maximum gamma-ray energy of 5.528 MeV via a head-on collision with a 746 ± 1 MeV electron beam in UVSOR-III [15]. The maximum energy of the LCS gamma-ray beam was increased to excite the $J^\pi = 1^-$ state at 5.512 MeV of ^{208}Pb because the NRF cross section is approximately twice larger than that at the 5.292-MeV level [24] measured in the previous experiment [16]. The spectral linewidth of the laser was 0.7 nm, while its beam quality M^2 was 1.05. The LCS gamma-ray flux before the collimator was estimated to be 10^8 photons/s with 100% energy bandwidth, which was ten times as large as that in the previous experiment (10^7 photons/s) [16].

We used a lead collimator with a hole diameter of 1 mm and a length of 20 cm. The beam diameters at the CT target and the witness target were approximately 1 mm because the divergence of the LCS beam is small (order of 10^{-3}). We obtained the 2-mm spatial resolution of NRF-CT images, defined by the scanning step of 2 mm as described previously. The EGS5 Monte Carlo simulation code [25] was used to evaluate the energy spectrum and flux of the LCS gamma rays at the CT target under the current experimental conditions. Fig. 6 shows the gamma-ray spectrum and the flux of the LCS gamma rays at the CT target under the current experimental conditions given by the EGS5 Monte Carlo simulation [25]. The flux of the LCS gamma-ray beam after the collimation was estimated to be 5.5 photons/eV/s at a maximum energy of 5.528 MeV with 1.1% energy bandwidth at the full-width at half-maximum (FWHM). The energy distribution shows typical features of the LCS gamma-ray beam, including a gradual increase at low energies and steep drop at high energies in the gamma-ray spectrum.

Fig. 7 illustrates the schematic of the experimental setup. A 5-mm-thick plastic scintillation detector was used to measure the flux of the incident LCS gamma-ray beam. The LCS gamma-ray beam was injected to the CT target following its traversal through the plastic scintillation detector. Subsequently, the gamma rays transmitted beyond the CT target were projected on the witness target constructed from the isotope of interest (^{208}Pb in purity $>97.8\%$). The diameter and the longitudinal length of the witness target were 6 and 12 mm, respectively. Two high-purity germanium (HPGe) detectors with efficiencies of 120% and 130% relative to a 3" $\times$ 3" NaI(Tl) scintillator were used to measure the NRF gamma rays from the witness target. These two HPGe detectors were placed at an angle of 120° with respect to the gamma-ray axis. The energy calibration of the HPGe detectors was performed with the ^{40}K (1460.8 keV) and ^{208}Tl (2614.5 keV) gamma rays from the natural background. The energy calibration was extrapolated to 5.512 MeV with a deviation of 2–4 keV which was verified by the 5.512-MeV peak as well as its single escape peak. The depth of the notch in the spectrum of the transmitted photon beam through the CT target induced by the isotope of interest was assessed based on the difference between the NRF yields obtained with and without the CT target. However, these NRF yields depend on the atomic attenuation in addition to the nuclear resonant attenuation in the CT target [26]. The transmission of the incident LCS gamma-ray photons through a target partly depends on the attenuation caused by atomic processes. A 3.5" $\times$ 4" $LaBr_3$(Ce) detector was used to measure the flux of the transmitted gamma rays to evaluate the atomic attenuation. Under the current experimental conditions, the total LCS gamma-ray flux was approximately 10^6 photons/s after the collimator. To prevent pile-up events in the $LaBr_3$(Ce) detector, a bismuth absorber (attenuator) with a thickness of 10 cm was placed in front of the detector. The dead times of all the detectors were less than 1%. The signals from each detector were sent to an eight-channel digital signal processor (APU8008, Techno-AP) and a conventional multichannel analyzer (MCA8000D, Amptek) which recorded all spectra. A flat panel detector was used to check the location of the gamma-ray beam and the CT target.

III. Results and Discussion

An NRF-CT image of the ^{208}Pb isotope placed inside an aluminum holder was obtained using gamma-ray transmission factor measurements, considering the atomic effect and attenuation of nuclear resonance. Fig. 8(a) and (b) shows the typical energy spectra measured with the $LaBr_3$(Ce) detector and the plastic scintillator. In each spectrum, the region of interest (ROI) is indicated by the shaded area. As seen in Fig. 8(a), the energy resolution of the $LaBr_3$(Ce) detector was high enough to separate between the LCS gamma-ray peak and its single escape, with the ROI covering the energy range of 5360–5885 keV to only include the full energy peak. In contrast, as illustrated in Fig. 8(b), the plastic scintillator exhibited a poor energy resolution, with no clear peak visible in the spectrum. Thus, the ROI covered the channels in the range of 817–7107 to obtain the relative flux of the incident LCS gamma rays.

For each measurement condition, the integrated count of the ROI was divided by the live time of the measurement system. The transmission factor (ε_{off}) of the OFF-resonance gamma

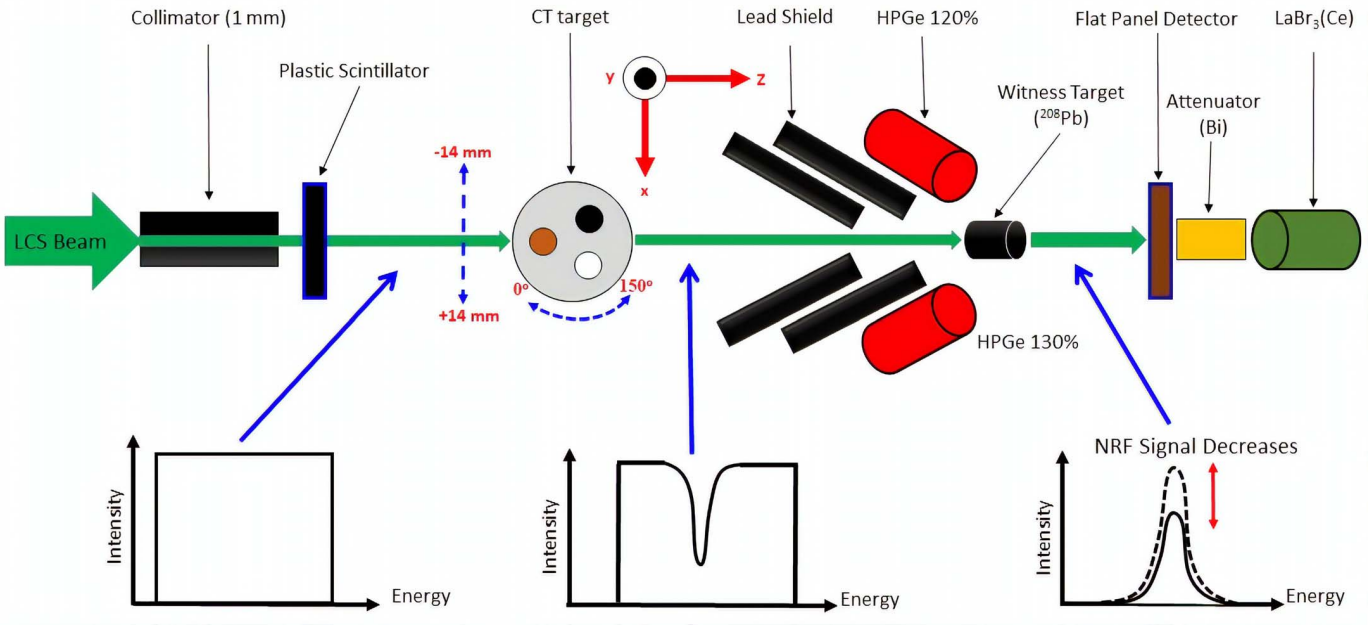

Fig. 7. Schematic of the NRF-CT experimental setup. A lead collimator with a diameter of 1 mm was employed. The setup included a plastic scintillator for calculating the gamma-ray flux from the incident LCS gamma-ray beam. The CT target was mounted on a 2-D motion stage placed in the path of the LCS gamma-ray beam. Two HPGe detectors were used for measuring the NRF signals from the witness target. Lead blocks were placed to shield the gamma rays directly dispersed onto the HPGe detectors. A flat panel detector was used to track the gamma-ray beams, while a bismuth attenuator (Bi), placed in front of the $LaBr_3(Ce)$ detector, prevented the pile-up of photons.

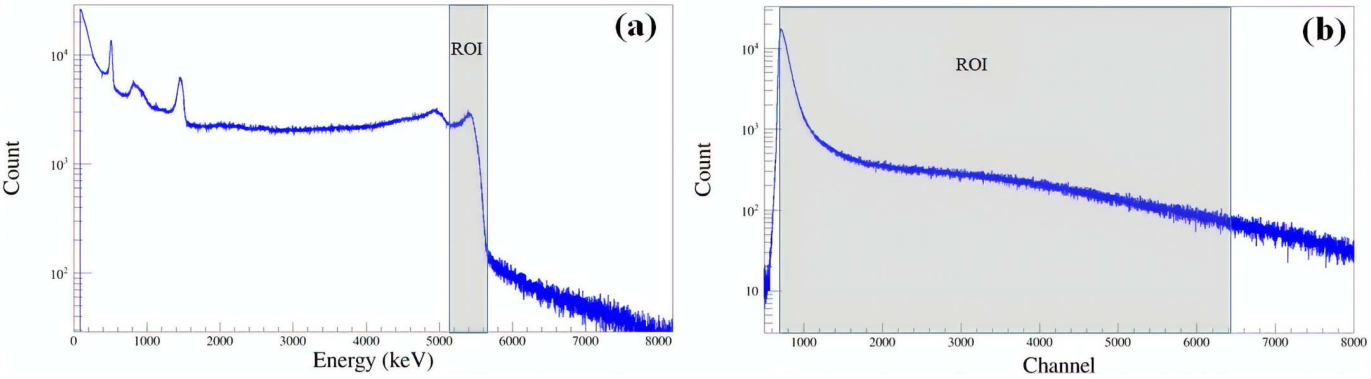

Fig. 8. Typical spectra from the $LaBr_3(Ce)$ detector whereas (a) the photo peak appears around 5512 keV and the bump in 511 keV before the photo peak is the single escape peak. (b) Typical spectra from the plastic scintillator. The shaded areas indicate the ROI in each spectrum.

ray for each measuring condition corresponding to the rotation angle (θ) and the horizontal position (x) of the CT target is given by [16]

$$\varepsilon_{\text{off}} = e^{\left[-\left(\frac{\mu}{\rho}\right)_{\text{ave}} \times \rho_{\text{ave}} \times L\right]}. \tag{1}$$

Here, $(\mu/\rho)_{\text{ave}}$ is the average mass attenuation coefficient, ρ_{ave} is the average density, and L is the length of the path through the target [16], [27]. This transmission (ε_{off}) is a function in the rotation angle (θ) and the horizontal position (x). The transmitted gamma rays were attenuated by the bismuth absorber; however, this absorption was canceled during the following treatment. To calculate the normalized count rate of the transmission detector, the count rate of the $LaBr_3(Ce)$ detector was divided by the total integrated count rate of the plastic scintillator. The transmission factor of the OFF-resonance gamma rays ε_{off} at each position can also be expressed by the following equation:

$$\varepsilon_{\text{off}} = \frac{C_{\text{off}}(\text{with CT target})}{C_{\text{off}}(\text{without CT target})}. \tag{2}$$

Here, C_{off} (with CT target) is the normalized count rate of the transmission detector in the presence of the CT target and C_{off} (without CT target) is the normalized count rate of the transmission detector in the absence of the CT target [16].

As the width of the ROI was wider than that of the NRF resonance by four to five orders of magnitude, the effect of resonance attenuation on the yield measured by the $LaBr_3(Ce)$ detector was negligible. To increase the statistics, the energy spectrum measured by each HPGe detector was compressed from 1 to 2 keV per channel along the energy axis, with the two compressed energy spectra subsequently summed to generate one spectrum. Fig. 9(a) displays the typical energy spectrum obtained by combining the two energy spectra

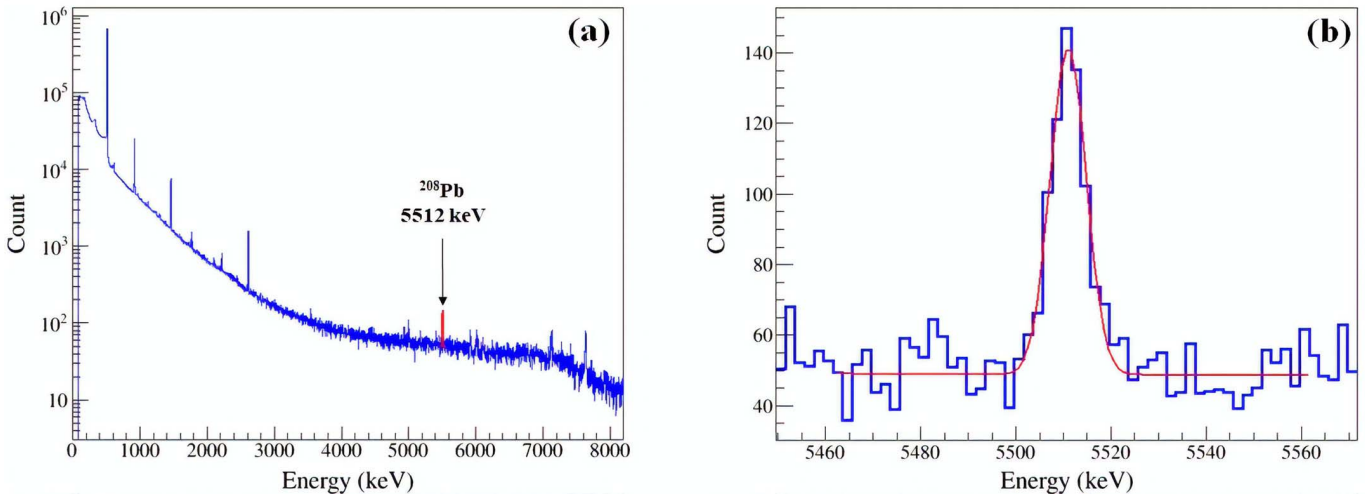

Fig. 9. (a) Combined spectrum from the two HPGe detectors. (b) Zoomed-in-view region shows a Gaussian fit of the NRF peak around 5512 keV.

measured using the two HPGe detectors. An NRF peak of ^{208}Pb was clearly observed at 5512 keV. Fig. 9(b) shows a zoomed-in plot of the region around the NRF peak. The FWHM values of the NRF peak corresponding to the 120% HPGe detector, 130% HPGe detector, and combined spectra were 7.6, 7.8, and 8.8 keV, respectively.

The NRF peak of ^{208}Pb at 5512 keV was fit with least-squares of the Gaussian function, with the NRF yield calculated based on the area under the peak. All data analyses were performed using the ROOT C++ codes [28]. The NRF yield was divided by the live time and normalized by the total count of the plastic scintillator detector; hence, the NRF yield can be considered as the normalized NRF count rate. The transmission factor ($\varepsilon_{\rm on}$) at the resonance energy for each measurement condition corresponding to the rotation angle (θ) and the horizontal location (x) of the CT target is given by [16]

$$\varepsilon_{\rm on} = e^{\left[-\left(\left(\frac{\mu}{\rho}\right)_{\rm ave} \times \rho_{\rm ave} \times L + \sigma_{\rm NRF} \times N_t\right)\right]}. \tag{3}$$

Here, $\sigma_{\rm NRF}$ is the NRF cross section of the isotope of interest and N_t is the areal density of the nuclide in the CT target in the LCS beam direction. This transmission ($\varepsilon_{\rm on}$) is a function of the rotation angle (θ) and the horizontal position (x). The transmission factor of the ON-resonance gamma rays $\varepsilon_{\rm on}$ at each position can also be expressed by the following equation:

$$\varepsilon_{\rm on} = \frac{C_{\rm on}(\text{with CT target})}{C_{\rm on}(\text{without CT target})}. \tag{4}$$

Here, $C_{\rm on}$ (with CT target) is the normalized NRF count rate obtained in the presence of the CT target and $C_{\rm on}$ (without CT target) is the normalized NRF count rate obtained in the absence of the CT target [16]. We assume that the attenuation of resonant photons originating from the atomic effect is the same as the attenuation of the beam photons. To obtain the NRF-CT image of the isotope of interest, we transformed the transmission factor to a logarithmic expression and evaluated the nuclear resonance attenuation $-\ln(\varepsilon_{\rm NRF})$ by subtracting the atomic attenuation according to the following equation [16]:

$$\ln(\varepsilon_{\rm NRF}) = \ln(\varepsilon_{\rm on}) - \ln(\varepsilon_{\rm off}). \tag{5}$$

In this study, the Algebraic Reconstruction Technique (ART) [29]–[31] was employed and details were written in [16]. Three 14 × 14 reconstructed images with a 2-mm pixel size were obtained. Fig. 10(a) displays the geometry of the CT target used in this study, while Fig. 10(b) shows the reconstructed image of the OFF-resonance attenuation measured by the $LaBr_3$(Ce) detector. The figure clearly shows two high attenuation areas caused by the atomic process corresponding to the positions of the ^{208}Pb and ^{206}Pb rods. As the intensities at the ^{208}Pb and ^{206}Pb rod positions measured based on atomic attenuation were nearly identical, it was practically impossible to distinguish between these two isotopes.

Fig. 10(c) displays the distribution of the ON-resonance gamma-ray attenuation, which was reconstructed from $\ln(\varepsilon_{\rm on})$ [defined in (4)]. While the ^{208}Pb rod could be clearly seen, the ^{206}Pb rod though visible exhibited a lower intensity than that of the ^{208}Pb rod. The absolute value of the ON-resonant attenuation [$-\ln(\varepsilon_{\rm on}) = 0.23$] at the ^{208}Pb rod position was approximately three times as high as that of the OFF-resonant attenuation [$-\ln(\varepsilon_{\rm off}) = 0.08$]. In contrast, the ON-resonant attenuation of $\ln(-\varepsilon_{\rm on}) = 0.08$ at the ^{206}Pb rod position was approximately identical to that of the OFF-resonant attenuation, implying that the ^{206}Pb intensity seen in Fig. 10(c) could be attributed to atomic attenuation. The reconstructed CT image obtained using (5) in Fig. 10(d) shows the distribution of the NRF attenuation induced only by the ^{208}Pb isotope (pure NRF). In the reconstructed image, the ^{206}Pb rod that is marginally visible in Fig. 10(c) is not visible in Fig. 10(d), while the ^{208}Pb rod can be clearly observed.

The present result shows that the NRF-CT method can clearly separate ^{208}Pb from ^{206}Pb and would be feasible to realize the isotope-specific CT imaging. We needed about 60 h to take the 2-D NRF-CT image of the sample in a diameter of 25 mm with a 2-mm pixel resolution. It should take nearly ten times longer acquisition time (600 h) to take 3-D NRF-CT image with the same CT target and pixel resolution. At least three or more higher order of intense gamma ray and a large number of detectors should be prepared in applications. Moreover, we should note that the current target NRF level ($J^\pi = 1^-$ state at 5.512 MeV) in ^{208}Pb

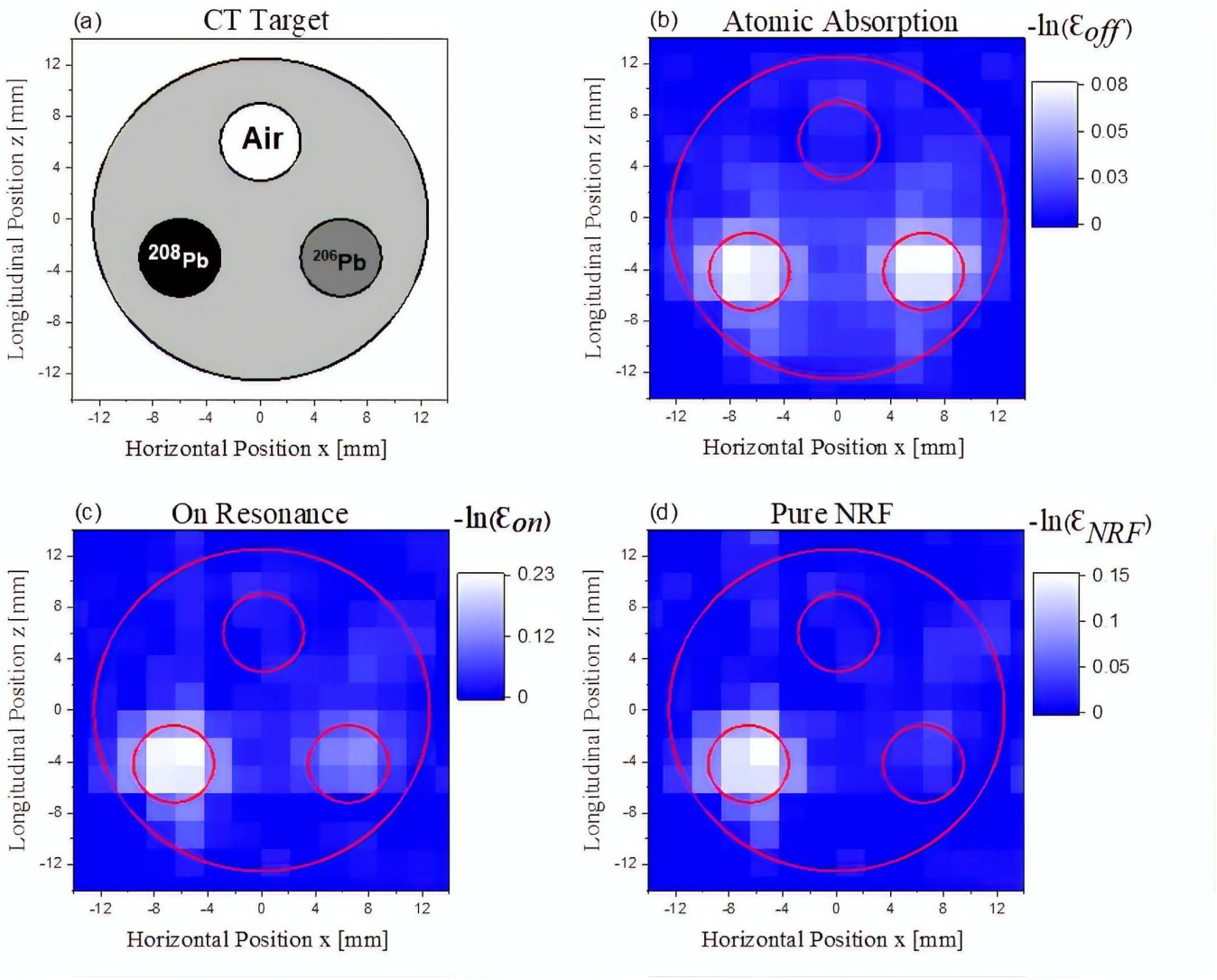

Fig. 10. (a) Geometry of the CT target. Reconstructed CT images of (b) atomic, (c) ON-resonance, and (d) pure NRF.

has a huge NRF cross section, $\Gamma_0 = 28.3$ [24], while a standard NRF level, that is, $J^\pi = 7/2^+$ state at 2.212 MeV in ^{27}Al ($\Gamma_0 = 17.1$ meV) [32] has three orders smaller NRF cross section. A new LCS gamma-ray facility is currently under construction in Extreme Light Infrastructure—Nuclear Physics (ELI-NP) [33], Romania. The LCS gamma-ray beam designed spectral density flux is within of 5×10^3 photons/s/eV range, which would be feasible for a practical application.

IV. Summary

In this study, the isotope selectivity of the NRF-CT technique was demonstrated for a CT sample where two different isotope-enriched rods (^{206}Pb in purity $>93.3\%$ and ^{208}Pb in purity $>97.8\%$) were installed in a thick aluminum holder for the first time. Both the isotope rods had an approximately the same atomic attenuation. The experiment was conducted using an LCS gamma-ray beam at the BL1U beamline of the UVSOR-III electron storage ring. By using a Tm-fiber laser system (50 W, CW) with 1.896-μm wavelength, the gamma-ray flux of 5.5 photon/s/eV and the maximum energy of 5.528 MeV LCS gamma-ray beam were generated. The CT sample was scanned by a 2-mm step size along the horizontal axes, from -14 to 14 mm, and a 30° step in the rotation angle from 0° to 150°. Reconstructed images with a 2-mm pixel size were obtained using an incident LCS gamma-ray beam with a diameter of 1 mm. Both the ^{208}Pb and ^{206}Pb rods were observed in the preliminary image owing to the atomic attenuation effect. The subtraction of the atomic attenuation effect eliminated the signal from the ^{206}Pb rod, resulting in the selective image of the ^{208}Pb isotope.

Acknowledgment

This work was performed at the BL1U of UVSOR Synchrotron Radiation Facility with the approval of Institute for Molecular Science (IMS), National Institute of Natural Science (NINS) (Proposal No. 19-503).

References

[1] W. Bertozzi and R. J. Ledoux, "Nuclear resonance fluorescence imaging in non-intrusive cargo inspection," *Nucl. Instrum. Meth. Phys. Res. B, Beam Interact. Mater. At.*, vol. 241, nos. 1–4, pp. 820–825, Dec. 2005, doi: 10.1016/j.nimb.2005.07.202.

[2] J. Pruet, D. P. McNabb, C. A. Hagmann, F. V. Hartemann, and C. P. J. Barty, "Detecting clandestine material with nuclear resonance fluorescence," *J. Appl. Phys.*, vol. 99, no. 12, Jun. 2006, Art. no. 123102, doi: 10.1063/1.2202005.

[3] R. Hajima, T. Hayakawa, N. Kikuzawa, and E. Minehara, "Proposal of nondestructive radionuclide assay using a high-flux gamma-ray source and nuclear resonance fluorescence," *J. Nucl. Sci. Technol.*, vol. 45, no. 5, pp. 441–451, May 2008. [Online]. Available: https://www.tandfonline.com/doi/abs/10.1080/18811248.2008.9711453

[4] T. Hayakawa *et al.*, "Nondestructive assay of plutonium and minor actinide in spent fuel using nuclear resonance fluorescence with laser Compton scattering," *Nucl. Instrum. Meth. Phys. Res. A, Accel. Spectrom. Detect. Assoc. Equip.*, vol. 621, nos. 1–3, pp. 695–700, Sep. 2010, doi: 10.1016/j.nima.2010.06.096.

[5] B. J. Quiter, B. A. Ludewigt, V. V. Mozin, C. Wilson, and S. Korbly, "Transmission nuclear resonance fluorescence measurements of ^{238}U in thick targets," *Nucl. Instrum. Meth. Phys. Res. B, Beam Interact. Mater. At.*, vol. 269, no. 10, pp. 1130–1139, May 2011, doi: 10.1016/j.nimb.2011.02.081.

[6] F. R. Metzger, "Resonance fluorescence of nuclei," *Progr. Nucl. Phys.*, vol. 7, pp. 54–88, Nov. 1959.

[7] G. Breit and E. Wigner, "Capture of slow neutrons," *Phys. Rev.*, vol. 49, no. 7, pp. 519–531, Apr. 1936, doi: 10.1103/PhysRev.49.519.

[8] J. R. Vavrek, B. S. Henderson, and A. Danagoulian, "Experimental demonstration of an isotope-sensitive warhead verification technique using nuclear resonance fluorescence," *Proc. Nat. Acad. Sci. USA*, vol. 115, no. 17, pp. 4363–4368, Apr. 2018, doi: 10.1073/pnas.1721278115.

[9] R. H. Milburn, "Electron scattering by an intense polarized photon field," *Phys. Rev. Lett.*, vol. 10, no. 3, pp. 75–77, Feb. 1963, doi: 10.1103/PhysRevLett.10.75.

[10] F. R. Arutyunian and V. A. Tumanian, "The Compton effect on relativistic electrons and the possibility of obtaining high energy beams," *Phys. Lett.*, vol. 4, no. 3, pp. 176–178, 1963, doi: 10.1016/0031-9163(63)90351-2.

[11] V. N. Litvinenko *et al.*, "Gamma-ray production in a storage ring free-electron laser," *Phys. Rev. Lett.*, vol. 78, no. 24, pp. 4569–4572, Jun. 1997, doi: 10.1103/PhysRevLett.78.4569.

[12] S. Miyamoto *et al.*, "Laser Compton back-scattering gamma-ray beamline on NewSUBARU," *Radiat. Meas.*, vol. 41, pp. S179–S185, Dec. 2006, doi: 10.1016/j.radmeas.2007.01.013.

[13] H. Ohgaki *et al.*, "Generation and application of laser-Compton gamma-ray at ETL," *Nucl. Instrum. Meth. Phys. Res. A, Accel. Spectrom. Detect. Assoc. Equip.*, vol. 455, no. 1, pp. 54–59, 2000, doi: 10.1016/S0168-9002(00)00693-8.

[14] N. Kikuzawa *et al.*, "Nondestructive detection of heavily shielded materials by using nuclear resonance fluorescence with a laser-Compton scattering γ-ray source," *Appl. Phys. Exp.*, vol. 2, Mar. 2009, Art. no. 036502, doi: 10.1143/APEX.2.036502.

[15] H. Zen *et al.*, "Generation of high energy gamma-ray by laser Compton scattering of 1.94-μm fiber laser in UVSOR-III electron storage ring," *Energy Proc.*, vol. 89, pp. 335–345, Jun. 2016, doi: 10.1016/j.egypro.2016.05.044.

[16] H. Zen *et al.*, "Demonstration of tomographic imaging of isotope distribution by nuclear resonance fluorescence," *AIP Adv.*, vol. 9, no. 3, Mar. 2019, Art. no. 035101, doi: 10.1063/1.5064866.

[17] T. A. Holly *et al.*, "Single photon-emission computed tomography," *J. Nucl. Cardiol.*, vol. 17, pp. 941–973, Jun. 2010, doi: 10.1007/s12350-010-9246-y.

[18] J. Kim, S. Jung, J. Moon, T. Kwon, and G. Cho, "Monte Carlo simulation for the design of industrial gamma-ray transmission tomography," *Prog. Nucl. Sci. Technol.*, vol. 1, pp. 263–266, Feb. 2011, doi: 10.15669/pnst.1.263.

[19] N. Estre, D. Eck, J.-L. Pettier, E. Payan, C. Roure, and E. Simon, "High-energy X-ray imaging applied to nondestructive characterization of large nuclear waste drums," *IEEE Trans. Nucl. Sci.*, vol. 62, no. 6, pp. 3104–3109, Dec. 2015, doi: 10.1109/TNS.2015.2498190.

[20] W. Bertozzi *et al.*, "Methods and systemic for computer tomography of nuclear isotopes using nuclear resonance fluorescence," U.S. Patent 8 180 019 B2, May 15, 2012. [Online]. Available: https://patentimages.storage.googleapis.com/a8/27/66/6d9ba9ef8b80e4/US8180019.pdf

[21] C. P. Barty *et al.*, "Overview of MEGa-ray-based nuclear materials management activities at the Lawrence Livermore national laboratory," Livermore Nat. Lab., Livermore, CA, USA, Tech. Rep. LLNL-CONF-515893, 2011.

[22] M. Adachi, H. Zen, T. Konomi, J. Yamazaki, K. Hayashi, and M. Katoh, "Design and construction of UVSOR-III," *J. Phys. Conf. Ser.*, vol. 425, no. 4, Mar. 2013, Art. no. 042013, doi: 10.1088/1742-6596/425/4/042013.

[23] T. Flohr, "CT systems," *Current Radiol. Rep.*, vol. 1, no. 1, pp. 52–63, Mar. 2013, doi: 10.1007/s40134-012-0005-5.

[24] J. Enders *et al.*, "Nuclear resonance fluorescence experiments on ^{204,206,207,208}Pb up to 6.75 MeV," *Nucl. Phys. A*, vol. 724, nos. 3–4, pp. 243–273, 2003, doi: 10.1016/S0375-9474(03)01554-9.

[25] H. Hirayama, "SLAC report number," Inter-Univ. Res. Inst. Corp., High Energy Accel. Res. Org. (KEK), Tsukuba, Japan, Tech. Rep. SLAC-R-730, 2005.

[26] H. Negm *et al.*, "A study of the nuclear resonance fluorescence reaction yield dependence on the target thickness of ^{208}Pb," in *NPNSNP*. Singapore: World Scientific, 2014, pp. 291–299, doi: 10.1142/9789814635455_0034.

[27] I. Daito, H. Ohgaki, G. Suliman, V. Iancu, C. A. Ur, and M. Iovea, "Simulation study on computer tomography imaging of nuclear distribution by quasi monoenergetic gamma rays with nuclear resonance fluorescence: Case study for ELI-NP application," *Energy Proc.*, vol. 89, pp. 389–394, Jun. 2016, doi: 10.1016/j.egypro.2016.05.051.

[28] M. Goto. (May 2018). *Root Data Analysis Framework*. [Online]. Available: https://root.cern.ch/root/htmldoc/guides/users-guide/ROOTUsersGuide.html

[29] R. Gordon, R. Bender, and G. T. Herman, "Algebraic reconstruction techniques (ART) for three-dimensional electron microscopy and X-ray photography," *J. Theor. Biol.*, vol. 29, no. 3, pp. 471–476, 1970, doi: 10.1016/0022-5193(70)90109-8.

[30] T. Sato, S. J. Norton, M. Linzer, O. Ikeda, and M. Hirama, "Tomographic image reconstruction from limited projections using iterative revisions in image and transform spaces," *Appl. Opt.*, vol. 20, no. 3, pp. 395–399, 1981, doi: 10.1364/AO.20.000395.

[31] J. Nuyts, B. De Man, J. A. Fessler, W. Zbijewski, and F. J. Beekman, "Modelling the physics in the iterative reconstruction for transmission computed tomography," *Phys. Med. Biol.*, vol. 58, no. 12, pp. R63–R96, Jun. 2013, doi: 10.1088/0031-9155/58/12/R63.

[32] P. M. Endt, "Energy levels of A = 21–44 nuclei (VII)," *Nucl. Phys. A*, vol. 521, pp. 1–400, Dec. 1990. [Online]. Available: https://www.sciencedirect.com/science/article/abs/pii/037594749090598G?via%3Dihub

[33] The ELI-NP Working Groups. *The White Book of ELI Nuclear Physics Bucharest-Magurele-Romania*. [Online]. Available: https://www.eli-np.ro/download.php